Induced stalled flow due to roughness sensitivity for thick airfoils in modern wind turbines

Gutiérrez, R.; Llorente, E.; Ragni, D.

DOI
10.1088/1742-6596/2151/1/012001

Publication date
2022

Document Version
Final published version

Published in
Journal of Physics: Conference Series

Induced stalled flow due to roughness sensitivity for thick airfoils in modern wind turbines

Induced stalled flow due to roughness sensitivity for thick airfoils in modern wind turbines

R Gutiérrez[1], E Llorente[1] and D Ragni[2]

[1]Nordex Energy Spain S.A.U, Avenida Ciudad de la Innovación 3, 31621 Sarriguren, Navarra, Spain.
[2]Aerodynamics, Wind Energy, Flight Performance and Propulsion Department, Faculty of Aerospace Engineering, Delft University of Technology, Kluyverweg 1, 2629, HS Delft, the Netherlands.

E-mail: RGutierrez@nordex-online.com

Abstract. The mid-span region of wind turbine blades can be thickened to fulfil the structural requirements of the blade. Hence, thick airfoils, that were designed to operate at the root region of the blade, are moved to the mid-span region. This could not imply remarkable variations of the blade performance once its surface is smooth. However, the sensitivity of thick airfoils to roughness could cause significant aerodynamic impacts such as flow separation. This research aims to quantify the impact of the blade thickness, under smooth and rough conditions, in the annual energy production and the fatigue loads of the blade. Ten blade designs, linearly interpolated in thickness, are studied employing aero-elastic computations. The results reveal that the thickest blade increases the annual energy production by 5% with respect to the thinnest blade under rough conditions. Whereas this increase is less than 1% under smooth conditions. The loss of annual energy production varies with the blade thickness linearly for thin blades while it varies exponentially for thick blades up to 22%. Fatigue loads assessment confirmed a reduction of the damage equivalent load under smooth conditions, whereas the thickest blade increased it 28% under rough conditions.

1. Introduction.

The surface roughness of wind turbine blades concerns wind turbine manufacturers from the characterization of the roughness on the blade [1] to the estimation of the wind turbine aerodynamic performance [2]. In parallel, the constant strive to extract more energy from the wind have encouraged blade designers to increase the length of wind turbine blades [3]. As explained by Jensen et al. [4], the weight of the blades should increase with blade length to the power of three. As a result, the effect of gravity and inertial loads gets dominant with respect to aerodynamic loading. Additionally, this increases the blade stiffness requirements necessary to withstand loads and keep tip deflection within limits.

One design approach for achieving the same level of stiffness with less material is to increase the thickness of the blade. The displacement of the spar cap from the neutral axis enhances the blade structural properties. However, this approach moves thick airfoils from the inboard blade region to the outboard one. Whereas the performance of smooth blades can be slightly affected, a significant impact can occur for rough ones. As explained by Timmer et al. [5], thick airfoils can provide with premature flow separation in case of leading-edge soiling. Consequently,

roughness sensitivity increases when thicker airfoils are required for the outboard sections of the blade.

For thin airfoils applications, roughness is known to decrease the maximum lift coefficient (C_{Lmax}), the slope of the lift coefficient C_L and increase the drag coefficient C_D [6]. Thick airfoils also suffer these aerodynamic impacts at high angles of attack [7]. However, Gutierrez et al. [8] measured an abrupt increase in C_L and C_D at low angles of attack which was caused by flow separation on the pressure side of a thick airfoil. This flow separation at low angles of attack was not previously reported in the literature because thick airfoils were designed to be insensitive to roughness at the high angles of attack of the root region. The use of thick airfoils in the mid-span region of the blade lowers the angle of attack (AoA) at which these airfoils operate. Consequently, the occurrences of flow separation on the blade pressure side can increase and influence the wind turbine performance. On the other hand, most of the studies about roughness impact on wind turbine performance, do not contemplate this kind of flow separation as they are mainly based on reporting Annual Energy Production (AEP) losses. Bak et al. [9] recently estimated an AEP loss of 5% for a 10 MW pitch controlled wind turbine.

This study aims to assess the influence of the blade thickness on the blade sensitivity to roughness.

2. Methods.

2.1. Description of sensitivity study.

This research carries out a sensitivity study to quantify the influence of the blade thickness on power production and fatigue loads of the blade for clean and rough conditions. For rough conditions some studies such as [28] and [29] assume the last 30% of the blade length to be eroded, this study assumes the last 50% to be rough. This decision is made to include the mid-span region of the blade in consideration. Even though, this could give a worst-case scenario in an erosion situation, other sources of roughness such as dirtiness could act at the mid-span region of the blade.

The relevant steps of this sensitivity study are shown in Figure 1.

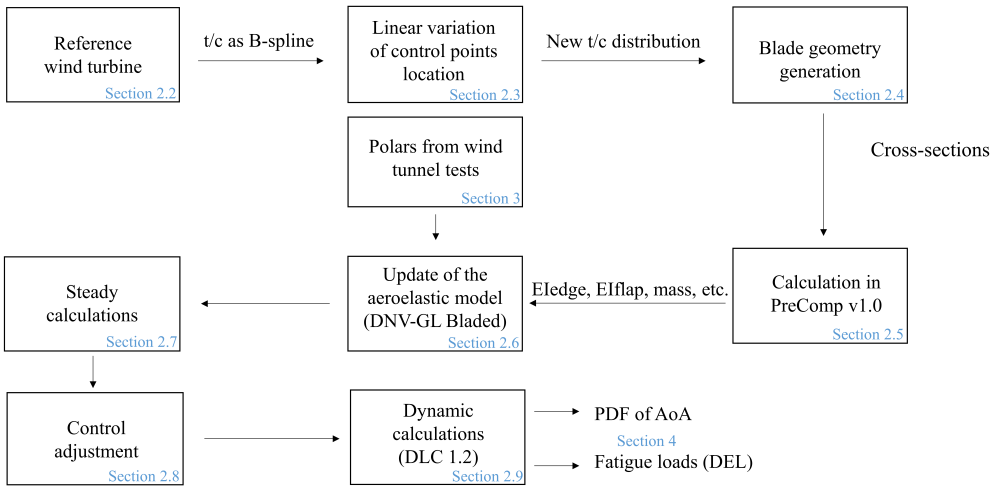

Figure 1: Sensitivity study procedure. The steps are related to the sections of this manuscript.

The variation of the t/c along a direction normal to the blade root (z or spanwise direction)

is expressed as a B-spline function. The location of the control points of the B-spline is varied to obtain a different t/c distribution. As a next step, the blade geometry is expressed as a B-spline surface. Several cross sections are extracted from this surface as a list of points. These sections are used in the PreComp v1.0 software to compute their structural properties. At this last step, the number of laminate layers is equal to the one of the reference wind turbine. This reference wind turbine is defined in section 2.2. The relative location of the internal blade structure remains the same and its elements are adapted to the new blade geometry. These two last simplifications ensure that the variations in the results only depend on the blade thickness. The description of the blade geometry and the cross-sectional structural properties of the blade are updated in the aeroelastic model defined in the DNV-GL Bladed software [17]. As a result of this process, aeroelastic steady calculations are carried out for a total amount of ten blades. Later, the gain K_λ and minimum pitch angle β_{pitch} are adapted to reduce the impact on AEP for these blades. This gain refers to the relation between the generator torque and the square of the angular velocity of the rotor, as shown in Equation 2. After assessing the tendency of the impact on AEP, three blades are selected as the most representative ones. Finally, dynamic calculations are performed for these blades providing results of fatigue loads as well as AoA probability density function (PDF).

The steps shown in Figure 1 are explained in the following sections.

2.2. Reference wind turbine

A pitch controlled multi-megawatt wind turbine is used in this study. The relevant parameters of the wind turbine are summarized in Table 1.

Quantity	**Value**	**Units**
Blade length (L)	75.8	m
P_{rated}	4.5	MW
Control type	Pitch feathering	
Hub height	120	m
Rotor diameter	155.18	m
Rotor Cone	5	deg
Rotor Tilt	5	deg
Transmission	Gearbox	
Rotor position	Upwind	
Cut-in	3	m/s
Cut-out	25	m/s
IEC Class	S	

Table 1: Wind turbine model description.

2.3. Linear variation of control points location.

This study takes the advantage of the affine invariance feature of B-splines [18]. The t/c distribution of the reference blade is expressed as a 1D parameterized curve in B-spline. The ordinates of the control points of this B-spline are contained in the vector Q. The values of Q are varied to define a different distribution. This variation is defined as a linear interpolation between two bounds (Equation 1). These bounds delimit the design space and were built from the t/c distribution of the reference wind turbine.

$$Q(F) = (1 - F) \cdot Q_{low} + F \cdot Q_{up} \tag{1}$$

where F is the interpolation factor defined between 0 and 1. This factor determines the similarity of the t/c distribution with the upper and lower bounds distributions. A null value of F implies a t/c distribution equal to the lower bound. Otherwise, a unit value of F corresponds to the upper bound. Q_{up} and Q_{low} are the ordinates of the upper and lower bounds, respectively.

These bounds have been defined according to:

- t/c values are restricted to be $\leq$ 30% for z/L $\geq$ 0.5. This decision is based on the lack of empirical data in the rough case for airfoils with t/c higher than 30%.
- The first fourth control points are not modified to conserve the same blade root diameter for all blades.

The F factor was varied to obtain ten blades used in steady calculations. Three of these blades were selected for dynamic calculations whose t/c distribution is shown in Figure 2a. Reference wind turbine blades [10],[11],[12] are inside the order of the t/c values of the design space for the outer half of the blade length.

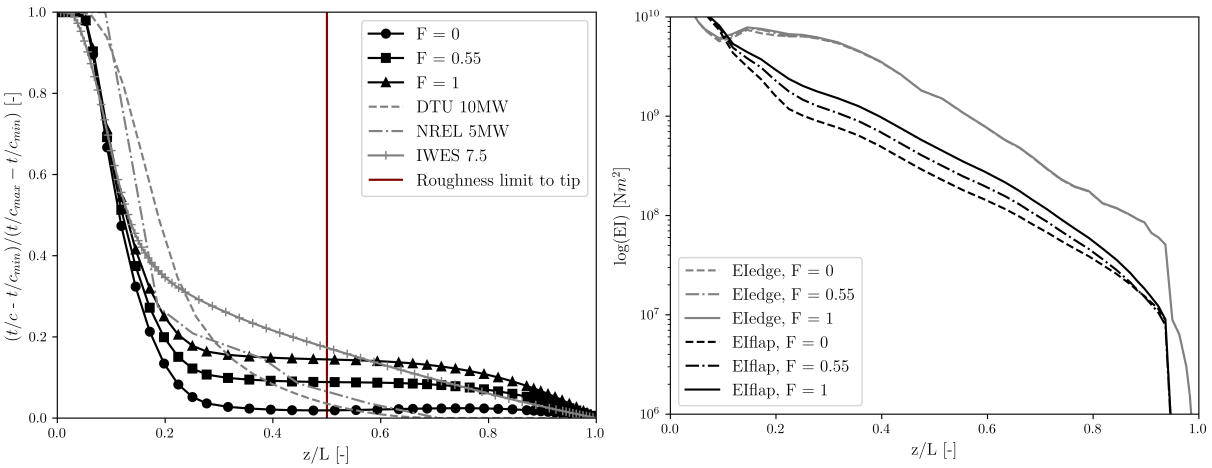

(a) Normalized relative thickness.

(b) Flapwise and edgewise stiffness.

Figure 2: Influence of the blade relative thickness on the stiffness of three blades of the study.

2.4. Blade geometry generation.

In this study, a set of predefined airfoils is transformed with respect to longitudinal distributions of the blade geometry variables. These distributions are expressed in B-spline form and determine the value along z of the t/c, the chord, the twist, the pre-bending and the relative airfoil location to z axis. This study refers to the predefined set of airfoils as master airfoils which are also treated in B-spline form. The t/c law dictates the location of these master airfoils and the cross-sectional variation between them. The t/c value at a precise z location is used as an interpolation factor for the cross-sectional variation between two consecutive master airfoils. Finally, the blade surface is expressed as a lofted B-spline surface [13].

2.5. Calculation in PreComp v1.0.

Cross-sectional structural properties are needed for the 1D Beam model used in Bladed [17]. PreComp v1.0 from NREL is the software chosen to perform the calculations of these properties. The code includes an analysis option to obtain blade properties such as bending stiffness, torsion stiffness, mass, moments of inertia, elastic–axis offset, and centre of mass offset along the blade

[16]. A two shear web configuration is used for the blade structure lay up of this study. The blade is assumed to be composed of different glass-fibre fabrics along with core materials infused in a matrix of epoxy resin. To study only the influence of the blade geometry on the results, the number of laminate layers per blade section is kept equal to the one used in the reference wind turbine.

Figure 2b compares the bending stiffness in flapwise and edgewise directions from PreComp calculations. According to [16], the EI_{edge} and EI_{flap} stiffness, are computed about a direction normal and parallel to the chord line of each section, respectively. The higher the F value is, the thicker the cross section is. Consequently, the laminate is relatively more displaced from the neutral axis and the stiffness is enhanced. This effect is notable from z/L values of 0.06 to 0.8. A higher increase of stiffness is given in the flapwise direction than in the edgewise direction.

2.6. Update of the aeroelastic model.
The new blade geometry description as well as the cross-sectional structural properties are specified in the aeroelastic model for a total number of 50 cross-sections. The polar data is specified only for the locations of the master airfoils. In this study, the aerodynamic coefficients data for intermediate values of t/c is interpolated with respect to the t/c value of two adjacent master airfoils.

For the rough blade cases, the specification of the aerodynamic data interpolation is adapted to fulfil the assumed roughness extension along the spanwise direction. As a result, clean and rough data are exchanged between the master airfoils depending on the t/c law. In Section 3, the empirical methodology, employed to extract this data, is explained.

For this study, the aerodynamic coefficients of the blade sections are determined for a Reynolds number (Re) of 3 million. This Re value corresponds to the maximum allowable value for the airfoil chord length and the wind tunnel explained in Section 3. The empirical data should be extrapolated in case of introducing the effect of Re variation with radial location and wind speed. However, there are no clear extrapolations to account for Re effect on the aerodynamic coefficients, especially for the rough conditions. The use of a wrong extrapolation would introduce more uncertainty into the study. A constant Re of 3 million along the blade, will provide with a worst-case scenario. But, variations between smooth and rough conditions are still valid because this Re assumption is used for both conditions.

2.7. Steady calculations.
Steady calculations are performed for uniform steady winds. Additionally, the deflections of the flexible blade components do not vary in time.

The result from these calculations is used to obtain the AEP of the ten studied blades. For the AEP calculation, a Weibull distribution is used with a shape factor k of 2 and an average wind speed at the hub height of 7.2 m/s.

2.8. Control adjustment.
The geometrical modification of the studied blades implies notable differences in structural properties such as a variation of the torsional stiffness and torsional flexibility. Hence, the range of operational angles of attack may differ and provide with power production losses with respect to the optimum performance. To overcome this impact, two basic control parameters, the gain K_λ and the minimum pitch angle β_{min}, are adjusted to ensure the maximum energy production per studied blade.

In regard to the Bladed theory manual [17], the demanded torque below rated power could be defined as:

$$T_g = K_\lambda \omega^2 \tag{2}$$

where K_λ is the gain and ω is the measured generator speed. This torque will maintain a desired tip-speed ratio λ and power production coefficient $C_p(\lambda)$.

Additionally, the power production below rated power depends on the minimum pitch variable β_{min}. This variable is a constant pitch value set for velocities lower than rated velocity. Above rated velocity, the pitch value is varied with respect to the pitch law.

Values of K_λ and β_{min} of 0.7 and 0 respectively are taken as a reference in clean calculations. However, an adjustement is done for rough cases to find the K_λ and β_{min} values that give the maximum AEP per blade design.

2.9. Dynamic calculations (DLC 1.2).

This study analyses the roughness impact on loads in terms of fatigue. Among the load cases described in IEC 61400-1 standard [15], DLC 1.2 cases are selected because they embody the requirements for loads that occur during the normal operation of a wind turbine throughout its lifetime. Specific situations such as start-up, shutdown and parked position are out of the scope of this research.

DLC 1.2 cases are defined by a normal turbulence model [15]. The wind speed standard deviation σ_1 is computed using the 90% quantile for a given hub height wind speed (V_{hub}) as suggested by the guideline. Consequently, for each wind speed, the turbulence intensity (TI) level is defined as σ_1/V_{hub}. Wind speed varies from 4 m/s to 24 m/s in steps of 2 m/s. Additionally, three yaw alignments, $-8°$, $0°$ and $8°$ are taken into account. A total number of 66 dynamic cases are computed with a simulation time per case of 10 minutes.

These cases are used to generate a stress history necessary to compute the cumulative damage of the wind turbine along its lifetime. The rainflow cycle counting subroutine of Bladed [17] is used to post-process the stress history. Finally, the computation of the damage equivalent load (DEL) is carried out for a wind turbine lifetime of 20 years.

3. Experimental database.

Available wind tunnel measurements focused on distributed roughness on airfoil leading edges (see Figure 3), are gathered to obtain the polar curves used in aero-elastic calculations for airfoils with t/c of 30%, 25% and 18%. The Reynolds number is 3 million for all the used experiments.

These aerodynamic measurements were carried out in the Low-Speed Lab Low-Turbulence Wind Tunnel (LSL-LTT) of the Delft University of Technology. LSL-LTT is an atmospheric tunnel of the closed-throat single-return type, with a contraction ratio of 17.8. It has a 2.9 m diameter six-bladed fan driven by a 525 kW DC motor, giving a maximum test section velocity of about 120 m/s. For all tests, a free stream velocity of 75 m/s was kept constant with a turbulence level of 0.07%. The test section is 1.80 m wide, 1.25 m high and 2.60 m long. Electrically actuated turntables flush with the test-section top and bottom walls positioned and supported a two-dimensional model in the middle of the test section length. All models were 1.25 meters long in the spanwise direction and 0.6 meters long in the chordwise direction. They were manufactured in resin infused glass fibre.

The angle of attack range is defined between $-20°$ and $20°$. A total number of 90 pressure taps were used on the models, to integrate the pressure component of the aerodynamic coefficients during 10 seconds of measuring time. The pressure taps orifices were at mid-span location and inclined to the incoming flow $15°$ to avoid the upstream influence of adjacent pressure taps. These orifices were more distributed on the airfoil leading-edge to retrieve the pressure gradient. A wake-rake of pitot tubes was installed downstream the airfoil to obtain total C_D based on the loss momentum method [19]. However, for angles of attack with flow separation, only pressure drag component C_{Dp} from pressure taps is used.

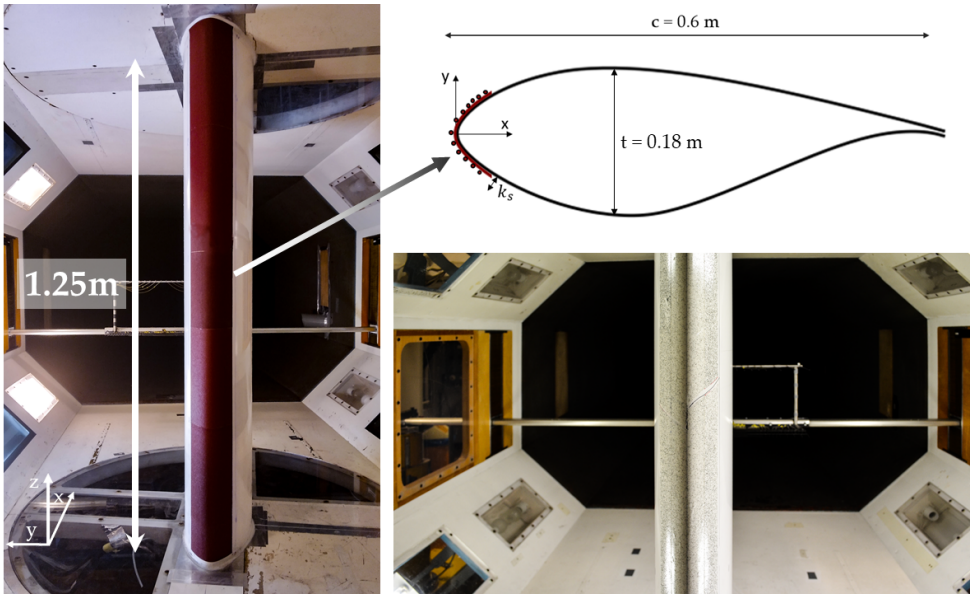

Figure 3: Sandpaper like roughness on the left and its drawing on top. Blown carborundum on the bottom right side.

3.1. Roughness emulation 25% and 18% thick airfoils.
To emulate the roughness state on the airfoil leading-edge, carborundum grains were blown on a double-sided tape. This tape was attached to the first 8%c on both airfoil sides following NACA standard method [6]. The grains density was ensured to be between 10% and 15% of the covered area. The normalized average grain height k_s/c was $4.67 \cdot 10^{-4}$ for both airfoils.

3.2. Roughness emulation 30% thick airfoil.
Sandpaper was used to emulate the roughness state on the airfoil leading-edge similarly to the work of Pires et al. [20]. The sandpaper was attached to the first 8%c on both airfoil sides. This sandpaper corresponded to an normalized average grain size (k_s/c) of $1.16 \cdot 10^{-3}$.

The main difference of this method with the 18% and 25% airfoil is the average grain height and density. Besides, sandpaper provides with a higher density of grains than the method of blown carborundum. On the other hand, another value of grain size is used.

It is important to remark that for all roughness states, no correlation is used in this study between the emulated roughness height and a roughness height found in a real wind turbine. The scientific community is researching this correlation [25], [23], [24]. The relatively higher value of k_s/c of the 30% thick airfoil, is combined with larger chords at the mid-span region of the blade. This would result in a higher k_s value than at outboards sections. As described by Wilcox et al. [26], thick airfoils collect larger regions of insect impingement due to the relatively lower impact velocity. In addition, Krisnhan et al. [27] demonstrated that insects which impact with high angles are less likely to smear over the surface. As a result, a higher height of attached particles is expected on the thick airfoils surface which is in concordance with the k_s/c value.

4. Results.

4.1. Empirical results.
The comparison of the variation of C_L and C_D, shown in Figure 4, shows that the thickest airfoil provides with the most significant C_D increase and C_L loss for positives angles of attack once the leading-edge gets rough. For angles of attack below 5°, the C_L and the C_D of the 30% airfoil

significantly increases compared to the other airfoils. For these low angles of attack the thick airfoil geometry generates an adverse pressure gradient that separates the flow on the airfoil pressure side under rough conditions. Figure 5 shows this flow separation for both an infrared thermography (IR) image and C_p measurements. The IR image corroborates the location of the flow separation. The cause of the increase in C_L and C_D is the plain C_p distribution measured from the 50% of the airfoil chord length to the trailing-edge. The consequences of the difference in aerodynamic coefficients are analyzed in Section 4.3.

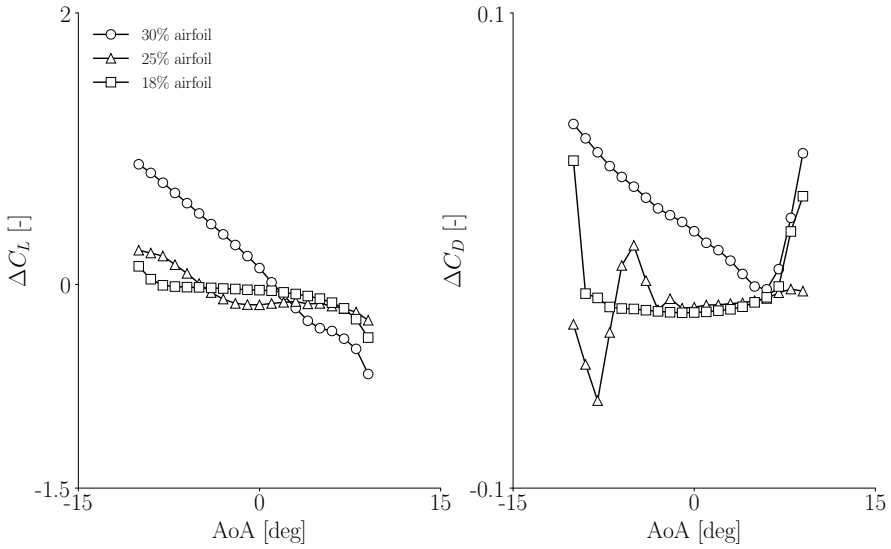

Figure 4: C_L loss and C_D variation with respect to smooth surface.

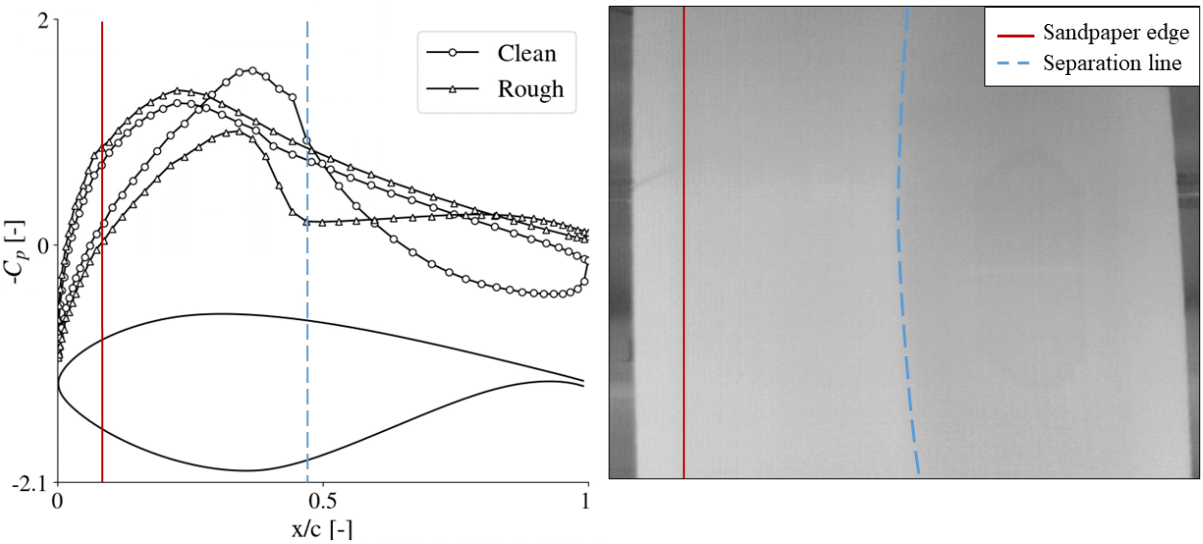

(a) Clean and rough C_p distributions.

(b) IR image on the rough airfoil pressure side.

Figure 5: Cross-check of the flow separation on the 30% thick airfoil at AoA of 0°.

4.2. Steady performance.
Figure 6 shows two different comparisons of the AEP. Figure 6a explains the impact of the increase in blade thickness for a given blade surface state (ΔAEP). This variable is computed with respect to the AEP of the thinnest blade (F = 0). The ΔAEP is at a maximum of 0.2 % in the smooth surface case, whereas, it abruptly changes in the rough case until a maximum value of 5%. The rough aerodynamic data of the 30% thick airfoil is used once the t/c value is 30% at the second half of the blade length. Blades with $F \geq 0.55$ fulfill this condition. This explains the abrupt change in the tendency from 1% to 5%. Consequently, the increase in blade thickness slightly varies the AEP under smooth surface conditions, whereas the AEP significantly varies under rough surface conditions.

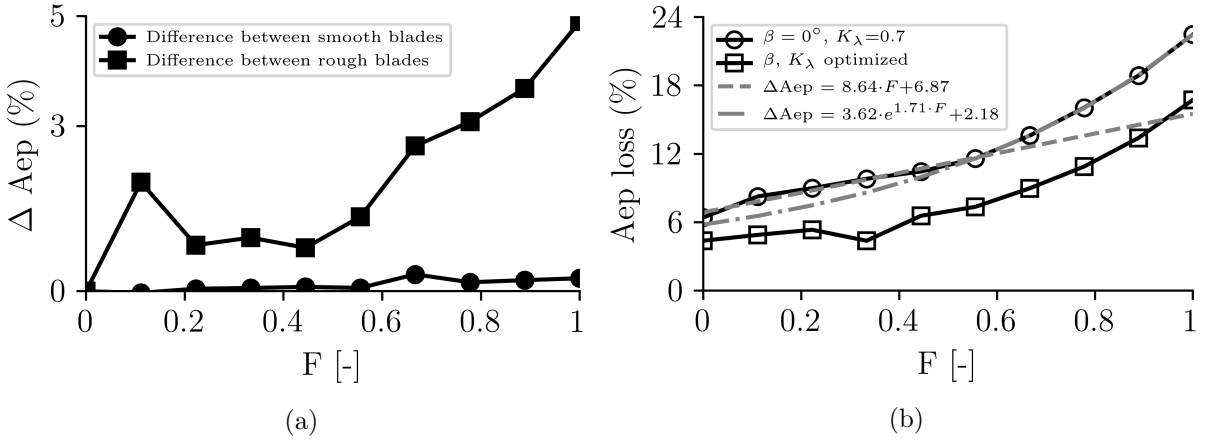

Figure 6: The AEP variation with respect to the thinnest blade of the study is shown in (a) per each surface condition. The AEP loss of each blade with and without control optimization is shown in (b).

Besides, Figure 6b shows the AEP loss per blade design with respect to smooth surface conditions. A linear tendency of the AEP loss with respect to blade thickness increase is shown until an F value equal to 0.55 is reached. From this value, the AEP loss changes to exponential tendency reaching values until 22% in the thickest blade design (F=1). Additionally, the optimization of K_λ and β_{min} explained in Section 2.8 reduces the AEP loss as an average of 5%.

4.3. Separated flow consequences.
In section 4.1, flow separation occurs at angles of attack $\leq 5°$ resulting in abrupt changes of the aerodynamic coefficients which can provide with an impact on blade operation. Hence, the angle of attack determines the necessary conditions for flow separation. Additionally, this flow condition only takes place for the 30% thick airfoil under rough conditions. It only occurs for blade designs in which the 30% thick airfoil relies on the outer half of the blade. This occurs for F values ≥ 0.55.

Due to the relation of the angle of attack with flow separation, the probability density function of the angle of attack is computed for different blade sections. Dynamic calculations are used to extract PDFs. This is done for three out of ten blades of the study. These blades are the thinnest blade (F = 0), an intermediate blade (F = 0.55) and the thickest blade (F = 1). Their t/c law can be seen in Figure 2. Figure 7 shows a higher variation of the maximum peak of the PDF for the thickest blade. The z/L section of value 0.43 is inside the smooth blade region and the other two are inside the rough one. The maximum peak is moved to the left in the rough

case with respect to the clean case. The likelihood of having separated flow is increased from F values higher than 0.55 as the maximum peak is around 5°. In contrast, the thinnest blade shows minimal variation in PDF distribution between surface states.

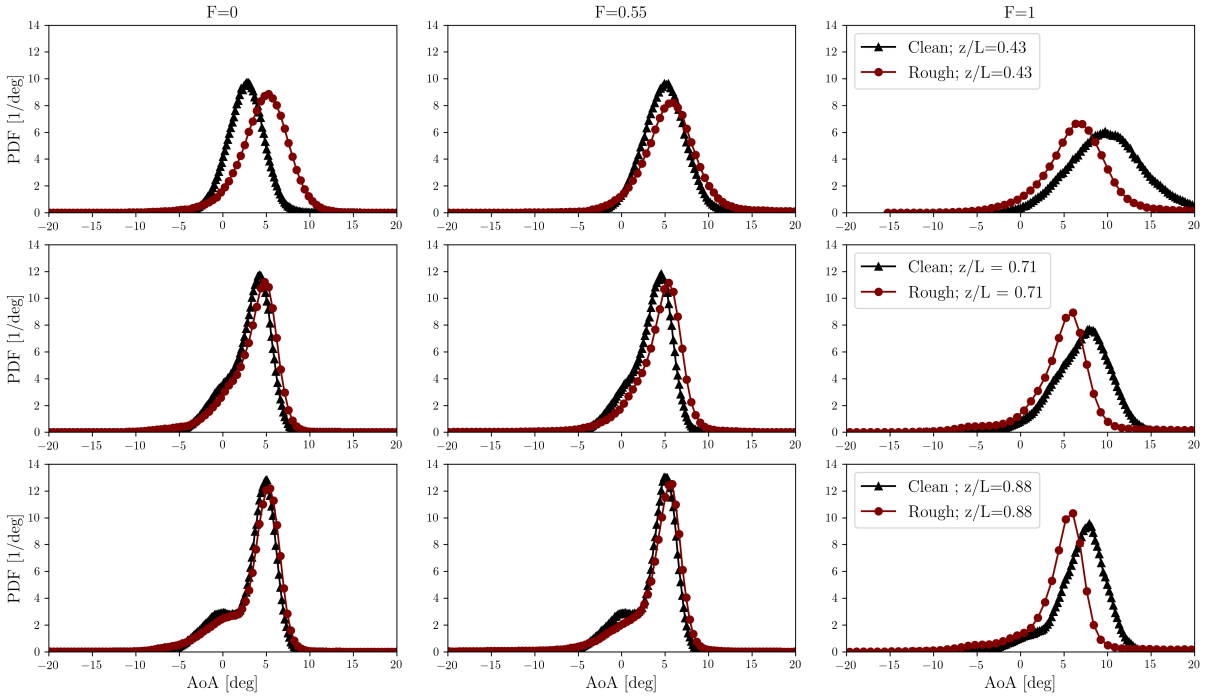

Figure 7: Probabilistic density functions (PDFs) for different relative blade locations z/L and F numbers.

After evaluating the probability of flow separation occurrence, its consequence is quantified by means of DELs. These loads were computed for three selected blade designs using the subroutine of Bladed software and the set-up described in section 2.9. As remarked by Papi et al. [28], the out-of-plane blade root bending moment M_{yroot} is a suitable indicator of overall blade loading. Additionally, the force F_{xroot} is relevant for the dimensioning of the root bearing. The x and y directions are defined normal and parallel to the chord line of each blade section, respectively. For the root section, x is parallel to the nacelle direction and y is normal to it. DELs are computed for M_{yroot} and F_{xroot} as these loads are related to the variation of EI_{flap} stiffness shown in Figure 2.

Figure 8 shows that the DEL of F_{xroot} is monotonically reduced in the clean case due to the effect of the blade thickness. This is related to the increase in blade stiffness shown in Figure 2. In contrast, the reduction of M_{yroot} is not monotonic but the thickest blade still provides with the lowest DEL value. For all blades, the rough surface state increases the DEL value with respect to clean blade condition. The thickest blade provides with the highest increment, 28% in F_{xroot} and 40% in M_{yroot}.

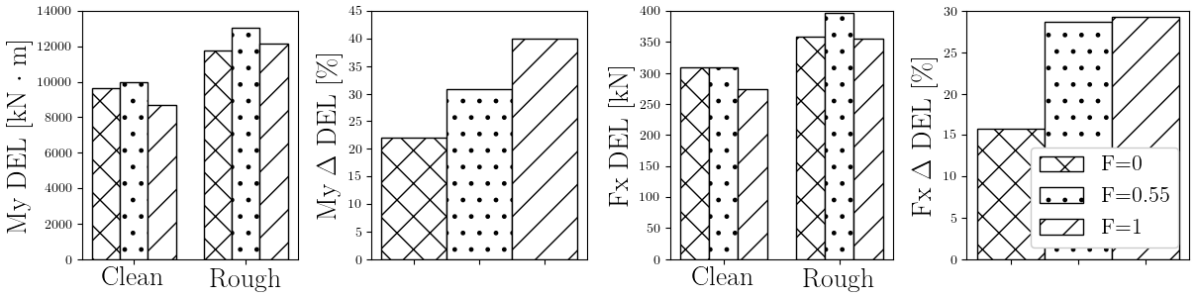

Figure 8: DEL comparison for 3 out of 10 blades of the studied. ΔDEL is computed with respect to clean value.

5. Conclusions.

This study quantifies these consequences in terms of AEP, DELs and likelihood of having flow separation in the case of thick blades.

Experimental data reveals that the 30% thick airfoil provides with notable sensitivity to roughness compared to 18% and 25% thick airfoils. Flow separation on the airfoil pressure side is given for angles of attack lower than 5° which is translated into a gain of lift and an increase of drag. The flow also separates in the 25% thick airfoil but for further negative angles of attack which are redundant for the analysed cases of power production.

It is demonstrated that ΔAEP slightly varies with blade thickness for smooth blades. Additionally, a DEL reduction due to blade thickness is also defined in clean conditions. As a result, the increase of blade thickness may be seen as a proper option for blade weight reduction. However, ΔAEP varies until 5% with respect to the thinnest blade under rough surface conditions. According to AEP loss, the 30% thick airfoil changes its tendency with blade thickness from linear to exponential until 22% of AEP loss. Finally, the optimization of K_λ and β_{min} parameters demonstrates a reduction of roughness impact on AEP loss.

The probable operational angle of attack range is demonstrated to be dependent on the surface roughness state. A damaged blade surface decreases the angle of attack range from the one defined in a smooth surface. Consequently, the probability of flow separation is increased due to the augmentation of the blade thickness.

For future blade designs, a balance should be found between the gain in stiffness and the risk of having flow separation consequences as well as AEP losses due to thick airfoil presence.

References

[1] Nielsen M. S. and Nikolov I. and Kruse E. K. and Garnaes J. and Madsen C. B. 2020 High-resolution structure-from-motion for quantitative measurement of leading-Edge roughness *Energies* **13** 3916.
[2] Kruse E. K. and Sørensen N. and Bak C. and Nielsen M. S. 2020 CFD simulations and evaluation of applicability of a wall roughness model applied on a NACA 633-418 airfoil *Wind Energy* **23** 2056–2067.
[3] Smil V. 2019 Wind Turbines Just Keep Getting Bigger, But There's a Limit. *IEEE Spectrum.*
[4] Jensen F. and Branner K. 2013 *Advances in Wind Turbine Blade Design and Materials* Woodhead Publishing Series in Energy: Number 47 (Cambridge UK) chapter 1 p 3
[5] Timmer W.A. and Bak C. 2013 *Advances in Wind Turbine Blade Design and Materials* Woodhead Publishing Series in Energy: Number 47 (Cambridge UK) chapter 4 p 118-146
[6] Abbott I.H. and von Doenhoff A.E. 2012 *Theory of Wing Sections: Including a Summary of Airfoil Data* Dover Publications (New York).
[7] Van Rooij R. P. J. O. M. and Timmer W. A. 2003 Roughness sensitivity considerations for thick rotor blade airfoils *J. Sol. Energy Eng. Trans. ASME* **125**(4) 468-478.
[8] Gutiérrez R and Llorente E. and Echeverría F. and Ragni D 2020 Wind tunnel tests for vortex generators mitigating leading-edge roughness on a 30% thick airfoil *J. Phys. Conf. Ser.* **1618** 052058.

[9] Bak C. and Forsting A. M. and Sorensen N. N. The influence of leading edge roughness, rotor control and wind climate on the loss in energy production *J. Phys. Conf. Ser.* **1618** 052050.
[10] Jonkman J. and Butterfield S. and Musial W. and Scott G. 2009 *Definition of a 5-MW Reference Wind Turbine for Offshore System Development* Technical Report NREL/TP-500-38060.
[11] Popko W. et al. 2018 *IWES Wind Turbine IWT-7.5-164 Rev 4* Fraunhofer Institute for Wind Energy Systems IWES. Bremerhaven.
[12] Bak C. et al. 2013 *Description of the DTU 10 MW Reference Wind Turbine.* DTU Wind Energy Report-I-0092
[13] Piegl L and Tiller W. 1995 *The NURBS Book. 2nd ed.* Springer Berlin, Heidelberg.
[14] Boor, C. 2001 *A Practical Guide to Splines. Applied Mathematical Sciences* Springer (New York).
[15] IEC 61400-1 Wind Turbines - Part 1: Design Requirements Edition 4 *IEC International Standards. International Electrotechnical Commission.*
[16] Gunjit S. B. 2005 User's Guide to PreComp *Tech. rep. Golden, CO: National Renewable Energy Laboratory.*
[17] Garrad Hassan & Partners Ltd Bladed Theory Manual Version 4.3 St Vincent's Works, Silverthorne Lane, Bristol BS2 0QD England.
[18] Farin G 2001 *Curves and Surfaces for CAGD. A Practical Guide 5th Edition.* Morgan Kaufmann Publishers San Francisco CA United States.
[19] Anderson J.D. 2010 *Fundamentals of Aerodynamics* McGraw-Hill Education (New York).
[20] Pires O and Munduate X and Boorsma K and Ceyhan O and Madsen H A. and Timmer W.A. 2018 Experimental investigation of Surface Roughness effects and Transition on Wind Turbine performance *Journal of Physics: Conf. Series* **1037** 052018.
[21] Mayes C. and Schlichting H. and Krause E. and Oertel H.J. and Gersten K. 2003 *Boundary-Layer Theory* Springer (Berlin, Heidelberg).
[22] Nikuradse, J. 1950 *Laws of flow in rough pipes* Tecnichal Memorandum 1292 National 26 Advisory Committe for Aeronautics Washington (USA).
[23] Bak C. and Gaunaa M. and Olsen S.A. and Kruse E. K. 2016 What is the critical height of leading edge roughness for aerodynamics? *J. Phys.: Conf. Ser.* **753** 022023.
[24] Mendez B and Muñoz A and Pires O and Munduate X 2017 *Characterization of the carborundum used in rough airfoil surface tests and modelling with CFD* 35th Wind Energy Symp. (Grapevine, Texas) 0916.
[25] Gaudern N. 2014 A practical study of the aerodynamic impact of wind turbine blade leading edge erosion *Journal of Physics: Conf. Series* **524** 012031.
[26] Wilcox B. and White E. 2016 Computational analysis of insect impingement patterns on wind turbine blades *Wind Energy* **19** pp 483–49.
[27] Krishnan K. and Robison R. and Tetteh E. and Loth E. and Farrell T. and Crouch J. and Berry D. 2016 *Characterization of insect residue on an aerodynamic leading edge* 8th AIAA Atmospheric and Space Environments Conference (Washington, D.C.) p 3445.
[28] Papi F and Balduzzi F and Ferrara G and Bianchini A 2021 Uncertainty quantification on the effects of rain-induced erosion on annual energy production and performance of a Multi-MW wind turbine. *Renewable Energy* **165** pp 701-715.
[29] Maniaci C. D. and Westergaard C. and Hsieh A. and and Paquette A. J. 2020 *J. Phys.: Conf. Ser.* **1618** 052082